Global Health & Medicine. 2024; 6(6):375-382.
ORIGINAL ARTICLE
DOI: 10.35772/ghm.2024.01058

Imaging of unicentric hyaline-vascular variant of Castleman disease: Emphasis on perilesional fat stranding and fatty proliferation

Sodai Hoshiai[1,*], Takeyuki Watadani[2,3], Shun Kagaya[4], Taishi Amano[4], Tomohiko Masumoto[5], Haruyasu Yamada[6], Izuru Matsuda[7], Ryota Matsuoka[8], Tetsuo Ushiku[9], Takahito Nakajima[1], Manabu Minami[1,5,6,7]

[1] Department of Radiology, Institute of Medicine, University of Tsukuba, Ibaraki, Japan;
[2] Department of Radiology, National Center for Global Health and Medicine, Tokyo, Japan;
[3] Department of Radiology, Graduate School of Medicine, The University of Tokyo, Tokyo, Japan;
[4] Department of Radiology, University of Tsukuba Hospital, Ibaraki, Japan;
[5] Department of Diagnostic Radiology, Toranomon Hospital, Tokyo, Japan;
[6] Department of Radiology, NTT Medical Center Tokyo, Tokyo, Japan;
[7] Department of Radiology, Kanto Rosai Hospital, Kawasaki, Kanagawa, Japan;
[8] Department of Diagnostic Pathology, Institute of Medicine, University of Tsukuba, Ibaraki, Japan;
[9] Department of Pathology, Graduate School of Medicine, The University of Tokyo, Tokyo, Japan.

Abstract: The hyaline-vascular variant of Castleman disease (HVCD) is relatively uncommon and demonstrates no specific clinical or laboratory findings; therefore, its preoperative diagnosis warrants a radiological evaluation. This study aimed to review imaging findings of HVCD, focusing on perilesional fat stranding and fatty proliferation. Patients with a pathologically confirmed HVCD diagnosis who had undergone CT were recruited from five hospitals from January 2000 to March 2023. Three experienced radiologists assessed CT findings, including lesion location, lesion size, calcification, enhanced pattern, feeding vessel visualization, and arterial enhancement. Perilesional fat stranding, fatty proliferation, neighboring fascial thickening, and surrounding lymphadenopathy were the primary targets of analysis. Moreover, the intensities and apparent diffusion coefficient (ADC) values on MRI and the maximum standardized uptake value (SUVmax) on ^{18}F-fluorodeoxyglucose positron emission tomography (PET) were evaluated. This study enrolled 43 patients (mean age 41.3 years ± 14.6 [standard deviation], 23 women). All lesions were well-defined round masses. Calcification and feeding vessels were detected in 21% (9/43) and 86% (36/43) of the patients, respectively. Perilesional fat stranding and fatty proliferation were observed in 44% (19/43) and 19% (8/43), respectively, with fatty proliferation detected only in retroperitoneal HVCD. Neighboring fascial thickening and surrounding lymphadenopathy were identified in 21% and 60%, respectively. The mean ADC value and SUVmax were 0.884×10^{-3} mm^2/s and 5.0, respectively. Retroperitoneal HVCD cases with perilesional fatty proliferation demonstrated a higher visceral fat ratio than those without ($p = 0.046$). Perilesional fat stranding and fatty proliferation were new characteristics of HVCD, especially in retroperitoneal cases.

***Keywords*:** Castleman disease, liposarcoma, fat, CT, MRI

Introduction

Castleman disease is a rare lymphoproliferative pathologic condition affecting lymph nodes and immune cells (*1*). It exists in two clinical forms: unicentric and multicentric. The former is usually asymptomatic, and its localization is restricted to a single node or nodal region. Meanwhile, the multicentric form typically manifests with general symptoms, such as fever, unintended body weight loss, fatigue, and appetite loss, as well as non-specific manifestations of anemia, multiple lymphadenopathies in several regions, and an enlarged spleen or liver. The two major histopathological types of Castleman disease are the hyaline-vascular and plasma cell variants. Previously, unicentric and multicentric forms corresponded to the former and latter types, respectively. However, some researchers currently believe that both histological types exist in each clinical form (*1*).

Several imaging features, particularly CT results, have been previously reported for the hyaline-vascular variant of Castleman disease (HVCD). These CT results included a solitary hypervascular round mass, well-defined margins indicating a noninvasive nature, calcification, especially arborizing shapes, and surrounding lymphadenopathies around the lesion (*2-11*). In addition, a clinical case of

HVCD masquerading as a dedifferentiated focus in a well-differentiated liposarcoma that demonstrated prominent fatty proliferation around a round mass was encountered. We have experienced similar cases in other hospitals, and PubMed research using the terms "Castleman[Mesh] AND fat[TIAB]" as of 9 June 2023 (time of presentation at a scientific meeting) and 30 April 2024 (time of manuscript preparation) has not yet reported these results well except for one case report (*12*).

The present study aimed to retrospectively analyze the imaging findings of unicentric HVCD in a large case series, mainly focusing on perilesional fat stranding and fatty proliferation.

Materials and Methods

Ethical approval

The institutional ethics review boards in five hospitals approved this multi-institutional study, which complied with the tenets of the Declaration of Helsinki and the Standards for Reporting Diagnostic Accuracy (*13*). Due to the retrospective design, they waived individual written informed consent.

Patient population

Patients were initially selected with a keyword search ("Castleman" and "CT or MR") in the radiological reporting systems from January 2000 to March 2023 in five hospitals. Data of patients with a pathologically confirmed Castleman disease diagnosis were retrieved. Inclusion criteria were surgically treated or biopsied unicentric lesions on CT. Exclusion criteria were nonpathologically confirmed cases, multicentric lesions on imaging, or absence of preoperative CT scans. Individuals with confirmed unicentric plasma cell variants were also excluded (Figure 1). Finally, preoperative CT findings of 43 cases with unicentric HVCD, including 42 surgically treated cases and one biopsied case, were analyzed. Preoperative MRI and positron emission tomography (PET) data, which were not indispensable, were evaluated. Patient demographics and clinical findings were extracted from respective hospital electronic records. Preoperative laboratory data, such as serum white blood cell (WBC) count, C-reactive protein (CRP), lactate dehydrogenase (LDH), and soluble interleukin-2 receptor (sIL2R), were analyzed.

Image acquisition and interpretation

CT imaging was conducted with 16–320-row multidetector systems (Mx8000 IDT 16, Brilliance 64, Philips Medical Systems, Best, Netherland; Aquilion, Aquilion Lightning, Aquilion ONE, Aquilion PRIME, Canon Medical System, Tochigi, Japan; LightSpeed QX/i, LightSpeed Ultra, Optima CT660, GE, Milwaukee, WI, USA; Emotion 6, Emotion 16, Siemens, Erlangen, Germany), including non-contrast examinations alone (n = 4), non-contrast and two-phase dynamic contrast (n = 12), non-contrast and three-phase dynamic (n = 12), non-contrast and portal venous phase contrast (n = 8), and portal venous phase contrast examinations alone (n = 7).

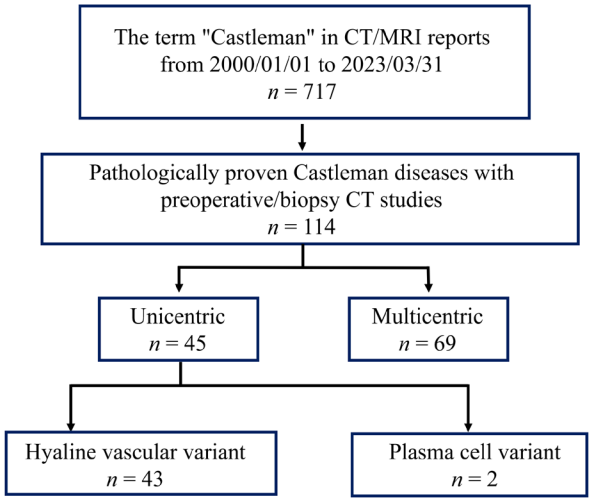

Figure 1. Flowchart of patient selection.

MRI was conducted in 22 patients with 1.5-T (n = 19) or 3-T machines (n = 3) (Achieva, Ingenia1, Ingenia 2, Philips Medical System; MAGNETOM Vision, MAGNETOM Spectra, Emotion 6, Skyra, Siemens, Signa Genesis, Signa HDxt, GENESIS Signa, GE; MRT200PP5, MRT100L2, Canon Medical System). Ten cases received contrast enhancement, including six with dynamic evaluations. One case underwent a dynamic contrast study with MRI alone. Diffusion-weighted images (DWI) and the apparent diffusion coefficient (ADC) values were obtained for 18 and 12 patients, respectively. Supplemental Table S1 (*https://www.globalhealthmedicine.com/site/supplementaldata.html?ID=94*) summarizes detailed scan parameters and contrast methods of CT and MRI studies.

Sixteen patients underwent PET/CT (Emotion Duo, Biograph64_mCT, Biograph16_TruePoint, Siemens; Aquiduo, Canon Medical System) after fasting for at least 10 h and receiving 3 MBq/kg of ^{18}F- fluorodeoxyglucose (FDG). Whole-body supine images were taken 90–120 min after ^{18}F-FDG injection, and the standardized uptake value (SUV) was determined in 15 cases.

Imaging analyses

Three experienced radiologists (S.H., T.W., and M.M., with 15, 21, and 40 years of experience in body imaging, respectively) independently evaluated CT and MRI images. Evaluated CT results reflected lesion location, maximum size, attenuation on non-contrast studies, calcification (arborizing, punctate, another shape, or none), enhanced pattern on portal venous phase

images of contrast-enhanced studies (homogeneous, inhomogeneous, or rim-like), and feeding vessels. Lesions' signal intensities were analyzed on T1WI, T2WI, and DWI in MRI studies. Flow void signals (intra-lesion, peri-lesion, both, or none) were estimated on T2WI. Vivid arterial or rim-like enhancements were observed during dynamic CT or MRI. Moreover, perilesional fat stranding, perilesional fatty proliferation (concentric pattern, eccentric pattern, or absent), neighboring fascial thickening, including abdominal peritoneal thickening, and surrounding lymphadenopathy, were analyzed on CT and MRI images. The outcomes in which agreement was achieved by two or more of the three radiologists were evaluated. The relevance of the findings was decided by a consensus in a case of disagreement among the three radiologists. Additionally, time-course changes in the lesion size were evaluated when multiple studies of CT and MRI were available preoperatively.

The ADC values of DWI on MRI and the maximum SUV (SUVmax) on ^{18}F-FDG-PET were determined by placing region-of-interest circles of the largest size possible to cover the lesion areas.

Visceral and subcutaneous fat volumes were calculated, to determine the relationship between perilesional fatty proliferation and visceral fat ratio (=visceral fat volume / (subcutaneous fat volume + visceral fat volume)), using medical image analysis software (AZE Virtual Place, Canon Medical System) in patients with retroperitoneal HVCD. Axial CT images obtained at the umbilical level were used for data analysis.

Statistical analysis

Mann–Whitney's *U*-test was used to evaluate the relationship of WBC, CRP, LDH, sIL2R, ADC values, and SUVmax with perilesional fat stranding and fatty proliferation. The difference between perilesional fatty proliferation and the visceral fat ratio was also evaluated in patients with retroperitoneal HVCD using the same test. Statistical Package for the Social Sciences (SPSS) for Windows version 26 (IBM SPSS Inc., Chicago, IL) was used for statistical analyses. *P*-values of < 0.05 indicated statistical significance.

Results

Patient characteristics and clinical findings

The study sample included 43 patients (mean age ± standard deviation: 41.3 ± 14.6 years, range: 16–77 years; 23 women).

All patients demonstrated preoperative serum WBC counts within normal limits. Serum CRP was elevated in three of them (5.7–16.4 mg/dL). Serum LDH levels were normal in all 41 patients with available data. Among 28 individuals in whom the measurements were performed, four patients showed increased serum sIL2R levels (571–1,190 U/mL).

Radiological findings

Among 43 lesions of HVCD, 16 (10 on the left side and 6 on the right), 14, 6, 4, 2, and 1 were located in the retroperitoneum, mediastinum, mesentery or mesocolon, neck, axilla, and chest wall, respectively. The mean diameter of lesions in HVCD was 4.4 ± 1.9 cm (mean ± standard deviation, range: 1.3–9.7 cm).

Table 1 summarizes the radiological findings of the enrolled patients. All lesions were homogeneously iso-attenuated to the skeletal muscle in 36 CT examinations, including non-contrast studies. All lesions analyzed in our study were a well-defined round soft-tissue mass. Calcification was detected in 9 (21%) of 43 patients, including arborizing configuration in 4 patients. Among 39 patients, enhanced patterns on portal venous phase contrast images were homogeneous in 31, inhomogeneous in 5, and rim-like enhanced in 3 patients. Cystic degeneration and necrotic changes were observed in five and two patients, respectively. Feeding vessels were visualized around lesions in 36 of 43 patients. Among all 22 patients that underwent MRI, none demonstrated hyperintense areas indicating hemorrhage on T1WI, and the obtained signal intensities on both T1WI and T2WI were comparable to those of lymph nodes. Flow void signals were detected inside the lesion in 5 of 22 patients, at the periphery encircling them in 9, and at both locations in 3 patients. The signal intensities on DWI were higher and similar to those of normal lymph nodes in 11 and 7 of 18 patients, respectively. All 25 lesions evaluated using dynamic CT or MRI were hypervascular in the arterial phase, and 6 of them demonstrated a rim-like enhancement.

Notably, 44% of the enrolled patients (19/43, Figures 2–6) and 75% of patients with retroperitoneal HVCD (12 of 16 cases) demonstrated perilesional fat stranding. Perilesional fatty proliferation was observed in 8 of 43 patients (19%), where all followed a concentric pattern. The eccentric pattern of perilesional fatty proliferation was not observed. All 8 lesions were located in the retroperitoneum (8 of 16 retroperitoneal cases, 50%; Figures 2–4), which was not characteristic of the other areas. Perilesional fat stranding was observed in all eight patients with perilesional fatty proliferation. Neighboring fascial thickening and surrounding lymphadenopathy were identified in 9 and 26 of the enrolled patients, respectively. The ADC value of 13 lesions was 0.884 ± 0.134 × 10^{-3} (mean ± standard deviation, range: 0.689–1.143 × 10^{-3}) mm^2/s.

The SUVmax of 15 lesions was 5.0 ± 3.5 (mean ± standard deviation, range: 2.1–16.3). The mean SUVmax value was 5.7 (n = 7) in patients with perilesional fat stranding and 4.4 (n = 8) in the opposite group; however, the Mann–Whitney *U*-test revealed no statistically

Table 1. Imaging findings in the hyaline-vascular variant of Castleman disease

	Overall (n = 43)	Retroperitoneum (n = 16)	Mediastinum (n = 14)	Mesentery/Mesocolon (n = 6)	Neck (n = 4)	Axilla/Chest wall (n = 3)
Calcification						
arborizing configuration	9% (4/43)	20% (3/16)	7% (1/14)	0	0	0
punctate	7% (3/43)	20% (3/16)	0	0	0	0
other shapes	5% (2/43)	7% (1/16)	7% (1/14)	0	0	0
none	79% (34/43)	53% (9/16)	86% (12/14)	100% (6/6)	100% (4/4)	100% (3/3)
Enhancement pattern on portal venous phase images						
homogeneous	79% (31/39)	86% (13/15)	64% (7/11)	100% (6/6)	75% (3/4)	67% (2/3)
inhomogeneous	13% (5/39)	7% (1/15)	36% (4/11)	0	0	0
rim-like enhancement	8% (3/39)	7% (1/15)	0	0	25% (1/4)	33% (1/3)
Visualization of feeding vessels						
present	84% (36/43)	97% (15/16)	86% (12/14)	83% (5/6)	50% (2/4)	67% (2/3)
absent	14% (6/43)	6% (1/16)	7% (1/14)	17% (1/6)	50% (2/4)	33% (1/3)
not assessable	2% (1/43)	-	7% (1/14)	-	-	-
Vivid arterial enhancement						
present	100% (25/25)	100% (12/12)	100% (8/8)	100% (5/5)	-	-
absent	0	0	0	0	-	-
Rim-like enhancement on arterial phase images						
present	24% (6/25)	33% (4/12)	0	40% (2/5)	-	-
absent	76% (19/25)	67% (8/12)	100% (8/8)	60% (3/5)	-	-
Flow void signals						
Present, intra-lesion	23% (5/22)	30% (3/10)	50% (2/4)	0	0	0
Present, peri-lesion	40% (9/22)	20% (2/10)	25% (1/4)	60% (3/5)	100% (2/2)	100% (1/1)
both	14% (3/22)	30% (3/10)	0	0	0	0
absent	23% (5/22)	20% (2/10)	25% (1/4)	40% (2/5)	0	0
Perilesional fat stranding						
present	44% (19/43)	75% (12/16)	29% (4/14)	50% (3/6)	0	0
absent	56% (24/43)	25% (4/16)	71% (10/14)	50% (3/6)	100% (4/4)	100% (3/3)
Perilesional fatty proliferation						
concentric pattern	19% (8/43)	50% (8/16)	0	0	0	0
eccentric pattern	0	0	0	0	0	0
absent	81% (35/43)	50% (8/16)	100% (14/14)	100% (6/6)	100% (4/4)	100% (3/3)
Neighboring fascial thickening						
present	21% (9/43)	31% (5/16)	14% (2/14)	33% (2/6)	0	0
absent	79% (34/43)	69% (11/16)	86% (12/14)	67% (4/6)	100% (4/4)	100% (3/3)
Surrounding lymphadenopathy						
present	60% (26/43)	62% (10/16)	64% (9/14)	50% (3/6)	50% (2/4)	67% (2/3)
absent	40% (17/43)	38% (6/16)	36% (5/14)	50% (3/6)	50% (2/4)	33% (1/3)

significant differences between the two groups (p = 0.613). Moreover, we found no evidence supporting the association of blood test findings and the ADC value with perilesional fat stranding. The mean SUVmax was 8.6 (n = 3) in the perilesional fatty proliferation group and 4.1 (n = 12) in the counterpart, indicating no remarkable differences in the outcomes of the performed Mann–Whitney U-test (p = 0.10). Blood test results and the ADC value did not significantly differ between the mentioned groups. The mean values of the visceral fat ratio in retroperitoneal HVCD cases with perilesional fatty proliferation and those without it were 0.46 (n = 8) and 0.33 (n = 8), respectively, demonstrating higher visceral fat ratios in the group showing perilesional fatty proliferation (p = 0.046).

Time-course changes in lesion size were evaluated for 23 patients. The average follow-up period was 28 months (range: 1–132 months). Seventy-four percent of lesions (17/23), exhibited no interval size changes, but five demonstrated an increase in size. Among them, one manifested a 2.9-fold increase, *i.e.*, from 1.8 cm to 5.3 cm over 3.5 years. The remaining one patient exhibited a decrease in lesion size from 3.7 cm to 3.0 cm over 7 years.

Discussion

Resection surgery is expected to treat unicentric Castleman disease completely, but accurate preoperative diagnosis of HVCD is essential to avoid an excessive intervention similar to that for malignant tumors (*1*). HVCD diagnosis is considered challenging because of its rarity, with no typical clinical symptoms, signs, or laboratory findings. The present study, including 43 cases, revealed no specific symptoms or laboratory findings associated with HVCD. Therefore, radiological evaluation is crucial for precise HVCD diagnosis.

The imaging findings of HVCD have been widely reported. Typical HVCD is incidentally detected in the neck, mediastinum, hilar region, mesentery, and

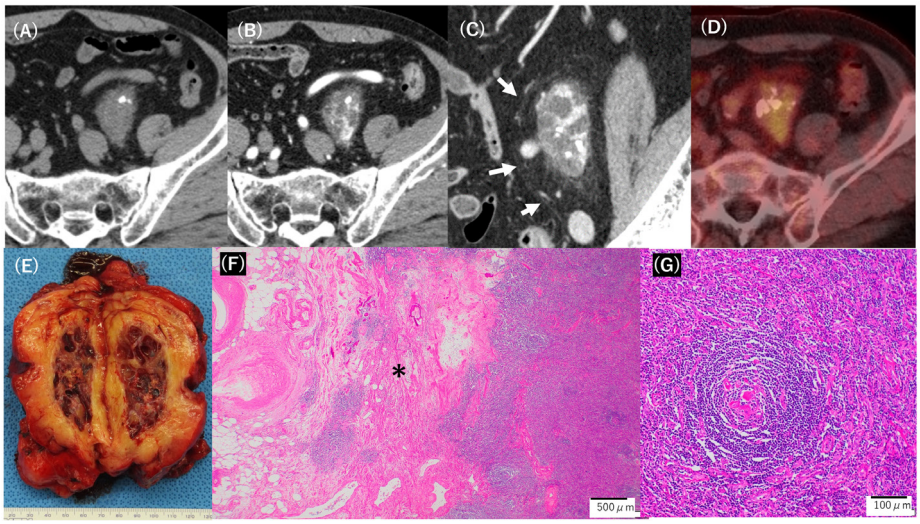

Figure 2. A 65-year-old man was admitted to our hospital due to the suspicion of retroperitoneal liposarcoma on CT before mycosis fungoides treatment. (A) In non-contrast CT, a 4.5-cm mass was observed in the left pelvic wall, which compressed the left external iliac artery anteriorly. **(B)** The mass showed a relatively strong heterogeneous contrast enhancement in contrast-enhanced CT with cystic degeneration inside. Coarse-to-nodular calcifications were observed within the mass. **(C)** The contrast-enhanced coronal MPR CT image revealed perilesional fat stranding and fatty proliferation, which were interpreted as a well-differentiated component of liposarcoma at the previous hospital. The parietal peritoneum of the pelvis was slightly thickened (arrows). **(D)** The mass was hypermetabolic, and the SUVmax was 4.49 in ^{18}F-FDG-PET /CT. **(E)** The mass and surrounding fatty tissue were removed *en bloc*. Grossly, the fat around the mass was white and hard, whereas the interior mass was reddish-brown. **(F)** Histological examination revealed fatty proliferation and dense fibrosis (*) around the mass. Lymph follicles with atrophied germinal centers and enlarged mantle zones were observed inside the mass. **(G)** Sclerotic blood vessels traversed into the germinal centers. Small vessel hypervascularization was observed between the follicles. Based on these findings, a diagnosis of hyaline-vascular Castleman's disease was made.

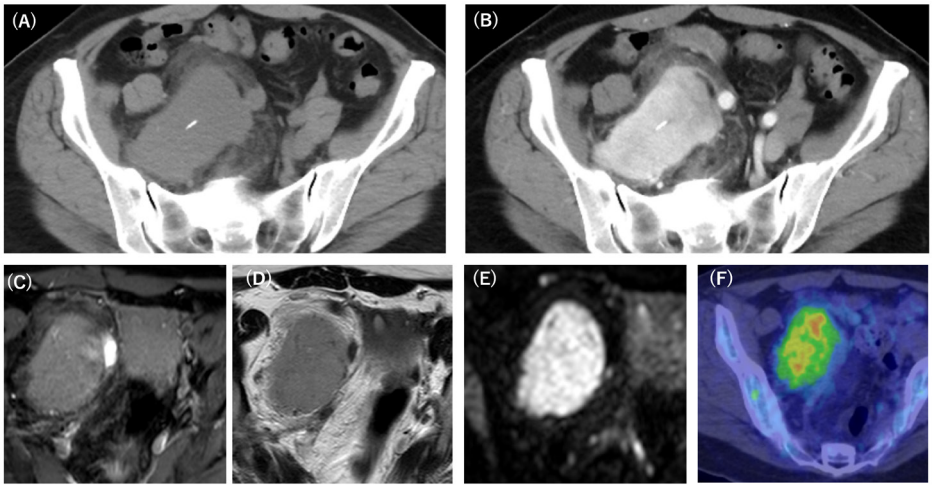

Figure 3. A 36-year-old woman was referred to our hospital because of a pelvic mass detected on an ultrasound examination for infertility. (A) A 9.0-cm mass was observed in the extraperitoneal space on the right side of the pelvis. A small linear calcification was observed in the center of the lesion. **(B)** Substantial contrast enhancement was identified in the mass on contrast-enhanced CT, accompanied by perilesional fat stranding and fatty proliferation. **(C)** Fat-saturated T1WI at the lower level of images **(A)** and **(B)** showed that the lesion had a signal equivalent to that of muscle. **(D, E)** The lesion was relatively hyperintense compared to muscle on T2WI and significantly hyperintense on DWI. The ADC value of the lesions was 0.985×10^{-3} mm^2/sec. **(F)** ^{18}F-FDG-PET/CT showed avid uptake of ^{18}F-FDG in the lesion. The mass was proven to be the hyaline-vascular variant of Castleman disease in pathological examinations.

retroperitoneum (*2*). It rarely occurs in the intestinal tract and abdominal parenchymal organs (*6,10*). It is usually diagnosed as a well-defined, round, solitary soft-tissue mass, with surrounding lymph node enlargement in 10.0%–54.5% of cases (*3,14*). Lesions are approximately 5.5 cm in diameter (*7*) and demonstrate relatively homogeneous attenuation on non-contrast CT, which is frequently comparable to skeletal muscle (*4*). The frequency of calcification is approximately 10%, which is not high, but discontinuous, coarse, and especially arborizing (dendritic)-shaped calcifications have been considered one of the characteristic imaging findings of HVCD (*2*). Contrast-enhanced CT shows abundant feeding vessels around lesions, with a strong and uniform

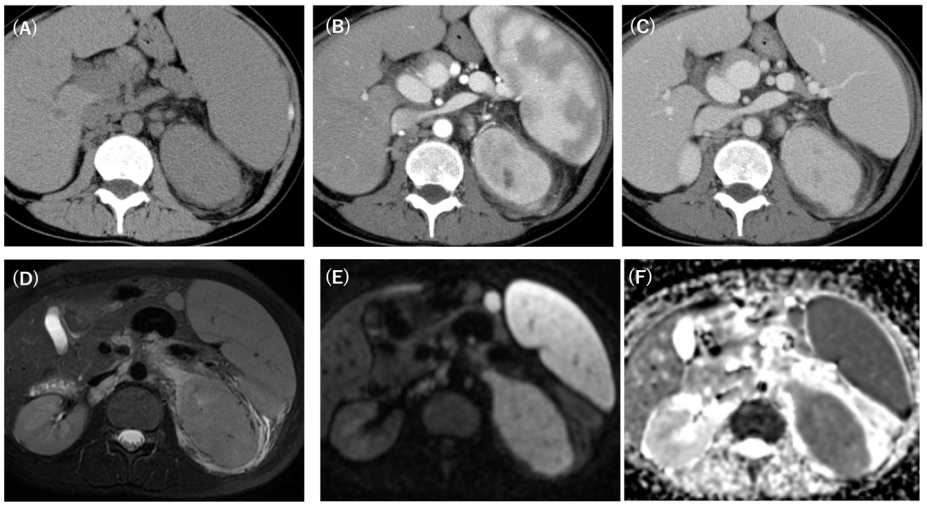

Figure 4. A 36-year-old woman with pathologically proven hyaline-vascular Castleman disease. (A) A well-defined 4.0-cm mass was identified in the retroperitoneum in front of the left psoas major muscle on non-contrast CT image. **(B)** The arterial phase image of dynamic contrast-enhanced CT showed hypervascularity with rim-like peripheral enhancement. **(C)** Portal venous phase image of contrast-enhanced CT displayed perilesional fat stranding and fatty proliferation. Thickening of the surrounding fascia was also observed. **(D)** The well-defined mass was almost isointense to the spleen, and high signal intensities, probably representing edematous changes, were observed around the lesion on fat-saturated T2WI. Encircling flow voids were noted around the mass. **(E)** DWI showed the mass of high signal intensities comparable to those of the spleen. **(F)** The ADC value of the lesion was 1.081×10^{-3} mm^2/sec.

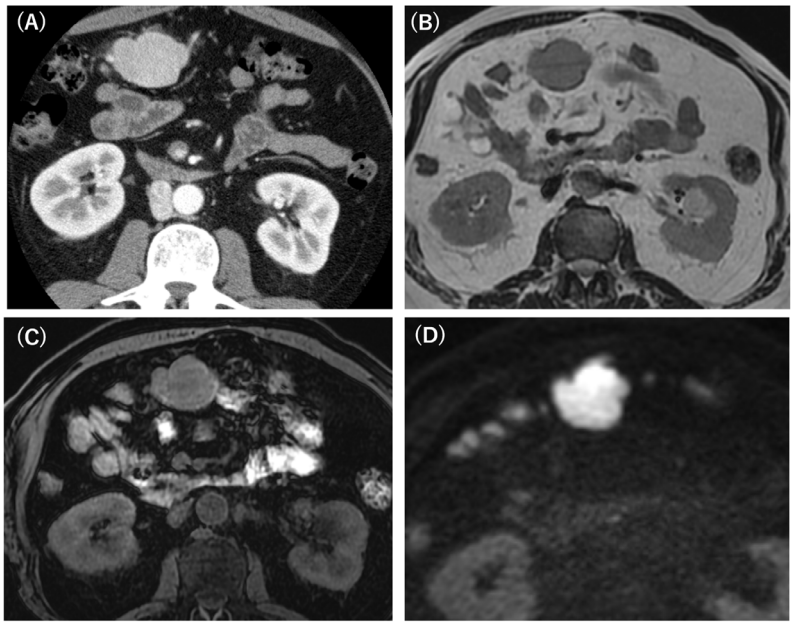

Figure 5. A follow-up CT scan of pancreatic intraductal papillary mucinous neoplasm revealed a 4.3-cm well-defined mass in the transverse mesocolon that was incidentally detected in a 49-year-old man. (A) The mass was homogeneously enhanced with perilesional fat stranding on contrast-enhanced CT. **(B)** T2WI revealed a slightly hyperintense mass compared to muscle and flow voids around it, probably due to feeding vessels. **(C, D)** The mass exhibited a similar signal to that of muscle on T1WI and markedly higher signal intensities on DWI.

contrast enhancement, but it can be heterogeneous in larger cases. Significantly, lesions of > 5 cm are heterogeneous, displaying internal fibrosis, necrosis, and degeneration (*3,7*). The signal intensity of the lesions is similar to or lower than that of a skeletal muscle on T1WI of MRI and is typically equal to or higher than that of a skeletal muscle on T2WI (*2,3,7*). The pattern of contrast effect on MRI is compatible with that seen on CT. In previous studies, feeding vessels were visualized within or around the lesion in 35.7%–51.2% of patients, which strongly indicated HVCD (*7,8*). Zheng *et al.* revealed a peripheral rim-like contrast effect in the arterial phase in three case series, where histological examinations in the peripheral portions of the tumors demonstrated increased small vessels (*15*). They reported fascial thickening around the retroperitoneal HVCD lesion in one of three

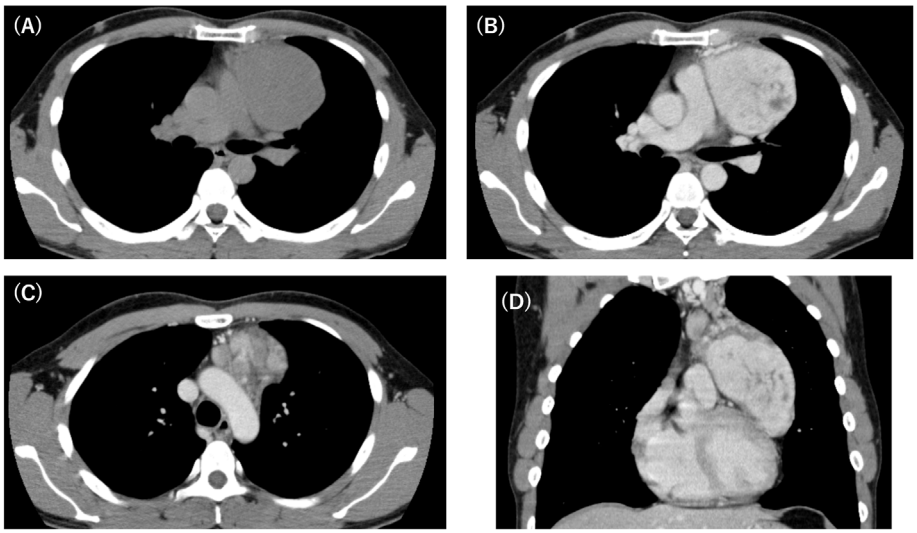

Figure 6. A 35-year-old man manifested a mediastinal mass on a chest radiograph for chickenpox. (A) A 9.7-cm mass was observed in the anterior mediastinum on non-contrast CT image. **(B)** The contrast enhancement of the mass was strong and heterogeneous. **(C, D)** Perilesional fat stranding with surrounding small lymphadenopathies was detected around the mass despite no evident fatty proliferation. The pathological diagnosis of the mass was a hyaline-vascular variant of Castleman disease.

cases (*15*). DWI revealed high signal intensities in all five cases reported by Zhao *et al.* (*7*). He *et al.* reveal avid ^{18}F-FDG uptake on PET/CT in all 18 patients in their study, with a median SUVmax value of 3.7 (2.4–5.2) (*16*).

These previously reported imaging findings were mostly consistent with the outcomes in this study. Well-defined round soft-tissue masses were observed in all evaluated cases. The frequency of calcification of the lesions was 21%, which was higher than that reported in previous studies. However, this may be associated with recent advances in CT, which enable higher spatial and contrast resolution and can be performed with thinner scanning techniques. The internal attenuation of the lesions was homogeneous in post-contrast evaluations in 79% of the assessed cases, and three cases demonstrated a rim-like enhancement. The signal intensities of lesions on T1WI, T2WI, and DWI of MRI were similar to those reported in previous studies. Feeding vessels were present around the lesions in 84% of the cases. Those who underwent dynamic studies demonstrated vivid arterial enhancement in all. Frequencies of rim-like enhancement in the arterial phase, flow void signals, and perilesional fascial thickening were not reported in previous studies, but the present study clarified these features and revealed that 60% of the cases were associated with surrounding lymphadenopathies. Meanwhile, ^{18}F-FDG accumulation rates were significantly not different from those reported in previous studies.

Perilesional fat stranding and fatty proliferation were not reported in previous studies. In the present study, perilesional fat stranding was observed in 75%, 29%, and 50% of the retroperitoneal, mediastinal, and mesentery lesions, respectively. Perilesional fatty proliferation was detected in 19% of the total cases, and 50% of the retroperitoneal lesions demonstrated perilesional fatty proliferation, but not in other body parts. All perilesional fatty proliferations had a concentric pattern. Perilesional fat stranding and fatty proliferation demonstrated no association with laboratory data, the ADC value on DWI, or the SUVmax on ^{18}F-FDG PET/CT. However, patients with a higher visceral fat ratio demonstrated perilesional fatty proliferation more frequently. The exact etiology of the indicated fat tissue changes is unknown. We speculate that mild chronic inflammation caused by HVCD may induce their development in obese patients. It is known that adipose tissue proliferates as a result of persistent weak chronic inflammation (*17*). The effect is more significant around lymph nodes because of the paracrine action between lymphoid tissue and surrounding adipose tissue (*18*). Chronic inflammation of the lungs and pleurae can cause thickening of subpleural fat, and chronic inflammatory diseases such as human immunodeficiency virus can cause hypertrophy of the omentum and mesentery (*18,19*). It is possible that HVCD, which involves lymphoid tissue, may have led to an increase in perilesional adipose tissue due to paracrine effects.

Previous studies revealed that the radiological differential diagnosis of HVCD included lymphoma, plasmacytoma, follicular dendritic cell sarcoma, soft-tissue sarcoma, thymic epithelial tumors and germ cell tumors in the mediastinum, gastrointestinal stromal tumors in the abdomen, and metastases (*2,4,9*). In dynamic studies, hypervascular lesions, such as paraganglioma, solitary fibrous tumor, and neuroendocrine tumor, were essential differential entities. Interestingly, the preoperative radiological differential diagnosis included liposarcoma in three of our eight

retroperitoneal cases with fatty proliferation. Perilesional fatty proliferation in HVCD forming concentrically around the lesions can be a differential point, whereas a dedifferentiated liposarcoma component is not always present in the center of the lesion, indicating an eccentric fatty proliferation in appearance (Supplemental Figure S1, *https://www.globalhealthmedicine.com/site/supplementaldata.html?ID=94*).

This retrospective study had several limitations. First, the imaging conditions were not uniform because it was conducted at five facilities having different technical settings. Second, most patients were racially homogeneous; therefore, the results of the present study may not be applicable to specific races due to different reported disease rates. Third, no comparative analysis was performed on differential diagnosis with other entities, especially dedifferentiated liposarcomas and hypervascular tumors, such as paragangliomas and solitary fibrous tumors. Further studies are warranted to address these aspects.

In conclusion, we reviewed the imaging findings of 43 patients with unicentric HVCD and identified perilesional fat stranding and fatty proliferation as new imaging characteristics. Radiologists should be aware that retroperitoneal HVCD may mimic dedifferentiated liposarcoma originating in a well-differentiated liposarcoma because of surrounding fatty proliferation.

Funding: None.

Conflict of Interest: The authors have no conflicts of interest to disclose.

References

1. Dispenzieri A, Fajgenbaum DC. Overview of Castleman disease. Blood. 2020; 135:1353-1364.
2. Bonekamp D, Horton KM, Hruban RH, Fishman EK. Castleman disease: The great mimic. Radiographics. 2011; 31:1793-1807.
3. Ko SF, Hsieh MJ, Ng SH, Lin JW, Wan YL, Lee TY, Chen WJ, Chen MC. Imaging spectrum of Castleman's disease. AJR Am J Roentgenol. 2004; 182:769-775.
4. Pitot MA, Tahboub Amawi AD, Alexander LF, LeGout JD, Walkoff L, Navin PJ, Kawashima A, Wood AJ, Dispenzieri A, Venkatesh SK. Imaging of Castleman disease. Radiographics. 2023; 43:e220210.
5. Zimmermann A. Hepatobiliary Castleman disease. In: Zimmermann A (ed) Tumors and Tumor-Like Lesions of the Hepatobiliary Tract: General and Surgical Pathology. Springer International Publishing. 2017; pp. 1729-1744.
6. Wang H, Wieczorek RL, Zenilman ME, Desoto-Lapaix F, Ghosh BC, Bowne WB. Castleman's disease in the head of the pancreas: Report of a rare clinical entity and current perspective on diagnosis, treatment, and outcome. World J Surg Oncol. 2007; 5:133.
7. Zhao S, Wan Y, Huang Z, Song B, Yu J. Imaging and clinical features of Castleman disease. Cancer Imaging. 2019; 19:53.
8. Lv K, Zhao Y, Xu W, Zhang C, Huang P. Ultrasound and radiological features of abdominal unicentric castleman's disease: A case series study. Medicine (Baltimore). 2020; 99:e20102.
9. Hill AJ, Tirumani SH, Rosenthal MH, Shinagare AB, Carrasco RD, Munshi NC, Ramaiya NH, Howard SA. Multimodality imaging and clinical features in Castleman disease: Single institute experience in 30 patients. Br J Radiol. 2015; 88:20140670.
10. Ergul E, Korukluoglu B, Yalcin S, Ozgun YM, Kusdemir A. Castleman's disease of the duodenum. J Pak Med Assoc. 2008; 58:704-706.
11. Li F, Xiao L, Cai H, Li L. Colonic Castleman disease on FDG PET/CT. Clin Nucl Med. 2023; 48:71-72.
12. Hakimi AA, Faiena I, Kaleya RN, Ghavamian R. Retroperitoneal Castleman's disease. Urology. 2010; 76:1379.
13. Bossuyt PM, Reitsma JB, Bruns DE, *et al.* STARD 2015: An updated list of essential items for reporting diagnostic accuracy studies. Radiology. 2015; 277:826-832.
14. McAdams HP, Rosado-de-Christenson M, Fishback NF, Templeton PA. Castleman disease of the thorax: Radiologic features with clinical and histopathologic correlation. Radiology. 1998; 209:221-228.
15. Zheng X, Pan K, Cheng J, Dong L, Yang K, Wu E. Localized Castleman disease in retroperitoneum: Newly discovered features by multi-detector helical CT. Abdom Imaging. 2008; 33:489-492.
16. He L, Chen Y, Tan X, Sun X, Zhang Q, Luo H, Jiang L. ^{18}F-FDG PET/CT and contrast-enhanced CT in the diagnosis of Castleman disease. Jpn J Radiol. 2023; 41:98-107.
17. Sadler D, Mattacks CA, Pond CM. Changes in adipocytes and dendritic cells in lymph node containing adipose depots during and after many weeks of mild inflammation. J Anat. 2005; 207:769-781.
18. Pond CM. Adipose tissue and the immune system. Prostaglandins Leukot Essent Fatty Acids. 2005; 73:17-30.
19. Santamarina MG, Beddings I, Lermanda Holmgren GV, Sanchez HO, Volpacchio MM. Multidetector CT for evaluation of the extrapleural space. Radiographics. 2017; 37:1352-1370.

Received July 26, 2024; Revised September 18, 2024; Accepted October 7, 2024.

Released online in J-STAGE as advance publication October 12, 2024.

**Address correspondence to*:
Sodai Hoshiai, Department of Radiology, Institute of Medicine, University of Tsukuba, 1-1-1 Tennodai, Tsukuba, Ibaraki 305-8575, Japan.
E-mail: hoshiai@md.tsukuba.ac.jp